JPE 9-4-6

Modeling of a Transfer Function for Frequency Controlled Resonant Inverters

Mu-Ho Han†, Chi-Hwan Lee*, and Woo-Hyun Kwon**

†Dept. of Mechanical & Electrical Engineering Research, RIST, Pohang, Korea
*Dept. of Electronics Eng., Uiduk University, Gyeongju, Korea
**Dept. of Electrical Engineering and Computer Science, Kyungpook National University, Taegu, Korea

ABSTRACT

A linear transfer function for the output current control of frequency-controlled resonant inverters is proposed in this paper. The circuit of resonant inverters can be transformed into two coupled circuits through the complex phasor transform. The circuits consist of cross-coupled power sources and passive elements. The circuits are used to induce the state space equation, which is transformed into the 4^{th} order cross-coupled transfer function. The 4^{th} order cross-coupled transfer function is modeled into a 2^{nd} order linear transfer function based on a behavior analysis of the pole and zero locations that facilitate a simple and intuitive linear transfer function. The feasibility and validity of the proposed linear transfer function were verified by simulation and experiment.

Keywords: Resonant Inverter, Complex Phasor Transform, Frequency Modulation

1. Introduction

Resonant inverters are usually structured to control the power by regulating either the input voltage at the AC terminal or the operating frequency. From the controller's perspective, the simplest and most stable method would be changing the operating frequency [1]. With the resonant inverter, the change of the operating frequency may control output current amplitude. However, it is not possible to acquire the transfer function because resonant inverters are modeled as a cross-coupled form [2][3][4]. Therefore, it is a general practice to select a current controller through experiments. If the resonant circuit is modeled by means of a general phasor transform, L and C are modeled as the reactive element and the complex resistance element. It is possible to make an equivalent circuit by using the complex phasor transform with modulated frequency. This equivalent circuit is very useful to simulate the envelope response [5][6][7][8][9][10]. It is difficult to obtain a transfer function directly by using a complex variable. Therefore, the bode diagram is obtained from the simulation result and the transfer function is determined indirectly [11][12][13].

Manuscript received January 15, 2009; revised April 17, 2009
†Corresponding Author: mhhan@rist.re.kr
Tel: +82-54-279-6752, Fax: +82-54-279-6888, RIST
Dept. of Mechanical & Electrical Eng., Research, RIST, Korea
*Dept. of Electronics Eng., Uiduk University, Korea
**Dept. of Electrical Eng., and Computer Science, Kyungpook National University, Korea

In this paper, we propose the linear transfer function of the frequency-controlled series resonant inverter based on the complex phasor transform. Through the complex phasor transform, a state space equation is acquired. The behavior of each variable is studied by simulating the state space equation. The linear frequency-to-output current transfer function is modeled based on the key observations of the pole and zero locations that facilitate a simple and intuitive linear transfer function. The feasibility and validity of the proposed linear transfer function are verified by Matlab simulations and experiments of an actual RLC series resonant circuit.

2. Circuit Description and Operation

Any analog modulated signal (AM, FM, or PM) can be described by the following general expression:

$$V_s(t) = V_1(t)\cos(\omega_c t) + V_2(t)\sin(\omega_c t) \tag{1}$$

Where $V_1(t)$ and $V_2(t)$ are the modulation signals and ω_c is the angular frequency of the carrier. (1) could also be written as

$$V_s(t) = \mathrm{Re}[(V_1(t) - jV_2(t))\exp(j\omega_c t)] \tag{2}$$

or as

$$V_s(t) = |V(t)|\,\mathrm{Re}[\exp(\arg(V(t))\exp(j\omega_c t)] \tag{3}$$

Where "arg($V(t)$)" is $\tan^{-1}(-V_2(t)/V_1(t))$. (3) implies that the modulated signal in the time domain $V_s(t)$ can be represented by a generalized phasor where both its magnitude and phase are time dependent. The expression of the complex phasor, $\vec{V}(t)$ and $\vec{I}(t)$ are

$$\vec{V}(t) = V_1(t) - j\cdot V_2(t)\ \ \vec{I}(t) = I_1(t) + j\cdot I_2(t) \tag{4}$$

The magnitudes of $\vec{V}(t)$ and $\vec{I}(t)$

$$\left|\vec{V}(t)\right| = \sqrt{V_1^2(t)+V_2^2(t)},\ \left|\vec{I}(t)\right| = \sqrt{I_1{}^2(t) + I_2{}^2(t)} \tag{5}$$

are equal to the modulation envelope of the original signal. The complex phasor representation can be used to drive the low frequency equivalent circuits that represent the envelope behavior of the system without involving the high frequency carrier. The general formula of the frequency-variable voltage source is assumed to be of this form.

$$V_s(t) = A\cos[\omega_c t + \frac{\beta}{\omega_m}\sin(\omega_m t)] \tag{6}$$

Where β and ω_m are the modulation index and modulation frequency respectively. The generalized voltage complex phasor is given in (7).

$$\vec{V}_s(t) = A\cos[\frac{\beta}{\omega_m}\sin(\omega_m t)] + jA\sin[\frac{\beta}{\omega_m}\sin(\omega_m t)] \tag{7}$$

From (4) and (7), we can obtain real and imaginary parts of voltage as follows :

$$V_1 = A\cos\left[\frac{\beta}{\omega_m}\sin(\omega_m t)\right],\ V_2 = -A\sin\left[\frac{\beta}{\omega_m}\sin(\omega_m t)\right] \tag{8}$$

Since the voltage source and current have been divided into the real and imaginary parts, the resonance current is also divided. The proposed methodology is demonstrated by considering the resonant circuit shown in Fig.1(a) driven by a modulated voltage.

In order to define the transfer function, the series resonant inverter is represented by the envelope equivalent circuit shown in Fig.1(b)[7]. The inductor, capacitor, and

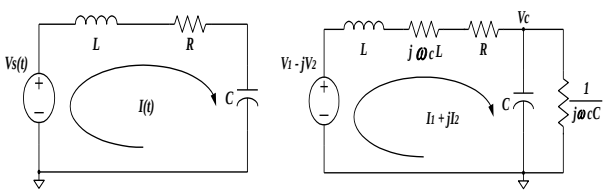

(a) Series resonant circuit. (b) Small signal phasor model.

Fig. 1. A resonant circuit and the equivalent circuit model.

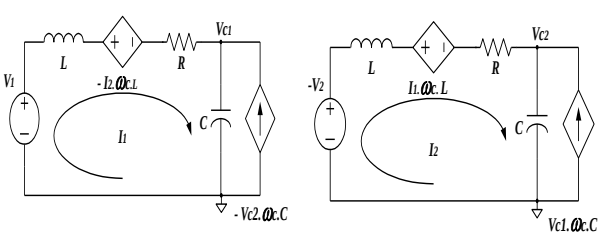

Fig. 2. An envelope equivalent circuit.

resistance are equivalently modeled by the phasor transform. Therefore, the cross-coupled equivalent circuit that considers the input elements $V_1(t)$ and $V_2(t)$, voltage sources $-I_2\omega_c L$ and $I_1\omega_c L$, current sources $-V_{c2}\omega_c C$ and $V_{c1}\omega_c C$ as well as R L C elements may be defined as in Fig.2.

The state space equation may be induced from the cross-coupled equivalent circuits as shown in Fig. 2 and represented in the following (9).

$$\begin{pmatrix} x_1' \\ x_2' \\ x_3' \\ x_4' \end{pmatrix} = \begin{pmatrix} -\frac{R}{L} & -\frac{1}{L} & \omega_c & 0 \\ \frac{1}{C} & 0 & 0 & \omega_c \\ -\omega_c & 0 & -\frac{R}{L} & -\frac{1}{L} \\ 0 & -\omega_c & \frac{1}{C} & 0 \end{pmatrix} \begin{pmatrix} x_1 \\ x_2 \\ x_3 \\ x_4 \end{pmatrix} + \begin{pmatrix} \frac{1}{L}V_1 \\ 0 \\ -\frac{1}{L}V_2 \\ 0 \end{pmatrix} \tag{9}$$

The output current equation is defined in the following (10)

$$\begin{pmatrix} I_1 \\ I_2 \end{pmatrix} = \begin{pmatrix} 1 & 0 & 0 & 0 \\ 0 & 0 & 1 & 0 \end{pmatrix} \begin{pmatrix} x_1 \\ x_2 \\ x_3 \\ x_4 \end{pmatrix} \tag{10}$$

where the state variable x_1 is defined as I_1, x_2 as V_{c1}, x_3 as I_2 and x_4 as V_{c2}.

3. Linear Transfer Function Induction

(9) and (10) can be converted to the transfer function. $I_1(s)$ and $I_2(s)$ could be written as (11) and (12). (11) and (12) can be expressed as the following equations (13) and (14) in order to observe the variation of the poles and zeros.

$$I_1(s) = \frac{1}{L}\left\{ \frac{8\omega_c\omega_o + \frac{R^2}{L^2}}{16\omega_c\omega_o} s - \frac{R}{4L}\frac{\omega_c}{\omega_o} + \frac{8\omega_c\omega_o - \frac{R^2}{L^2}}{16\omega_c\omega_o} s + \frac{R}{4L}\frac{\omega_c}{\omega_o} \right\} V_1(s)$$

$$-\frac{1}{16\omega_o L}\left\{ \frac{\frac{4R}{L}s + 8\omega_o^{\,2} + \frac{R^2}{L^2} + 8\omega_c\omega_o}{(s+\frac{R}{2L})^2 + (\omega_c+\omega_o)^2} - \frac{\frac{4R}{L}s + 8\omega_o^{\,2} + \frac{R^2}{L^2} - 8\omega_c\omega_o}{(s+\frac{R}{2L})^2 + (\omega_c-\omega_o)^2} \right\} V_2(s) \tag{11}$$

$$I_2(s) = -\frac{1}{L}\left\{ \frac{8\omega_c\omega_o + \frac{R^2}{L^2}}{16\omega_c\omega_o} s - \frac{R}{4L}\frac{\omega_c}{\omega_o} + \frac{8\omega_c\omega_o - \frac{R^2}{L^2}}{16\omega_c\omega_o} s + \frac{R}{4L}\frac{\omega_c}{\omega_o} \right\} V_2(s)$$

$$-\frac{1}{16\omega_o L}\left\{ \frac{\frac{4R}{L}s + 8\omega_o^{\,2} + \frac{R^2}{L^2} + 8\omega_c\omega_o}{(s+\frac{R}{2L})^2 + (\omega_c+\omega_o)^2} - \frac{\frac{4R}{L}s + 8\omega_o^{\,2} + \frac{R^2}{L^2} - 8\omega_c\omega_o}{(s+\frac{R}{2L})^2 + (\omega_c-\omega_o)^2} \right\} V_1(s) \tag{12}$$

$$I_1(s) = \frac{1}{L}\left\{\frac{As-B}{M_1(s)} + \frac{Cs+B}{M_2(s)}\right\} V_1(S) - \frac{1}{16\omega_o L}\left\{\frac{Ds+E}{M_1(s)} - \frac{Ds+F}{M_2(s)}\right\} V_2(s)$$

$$= \frac{1}{L}\{F_1(s)+F_2(s)\} V_1(s) - \frac{1}{16\omega_o L}\{F_3(s)-F_4(s)\} V_2(s) \tag{13}$$

$$I_2(s) = -\frac{1}{L}\left\{\frac{As-B}{M_1(s)} + \frac{Cs+B}{M_2(s)}\right\} V_2(S) - \frac{1}{16\omega_o L}\left\{\frac{Ds+E}{M_1(s)} - \frac{Ds+F}{M_2(s)}\right\} V_1(s)$$

$$= -\frac{1}{L}\{F_1(s)+F_2(s)\} V_2(s) - \frac{1}{16\omega_o L}\{F_3(s)-F_4(s)\} V_1(s) \tag{14}$$

where $A = \frac{8\omega_c\omega_o + \frac{R^2}{L^2}}{16\omega_c\omega_o}$, $B = \frac{R}{4L}\frac{\omega_c}{\omega_o}$, $C = \frac{8\omega_c\omega_o - \frac{R^2}{L^2}}{16\omega_c\omega_o}$, $D = \frac{4R}{L}$, $E = 8\omega_o^{\,2} + \frac{R^2}{L^2} + 8\omega_c\omega_o$, $F = 8\omega_o^{\,2} + \frac{R^2}{L^2} - 8\omega_c\omega_o$.

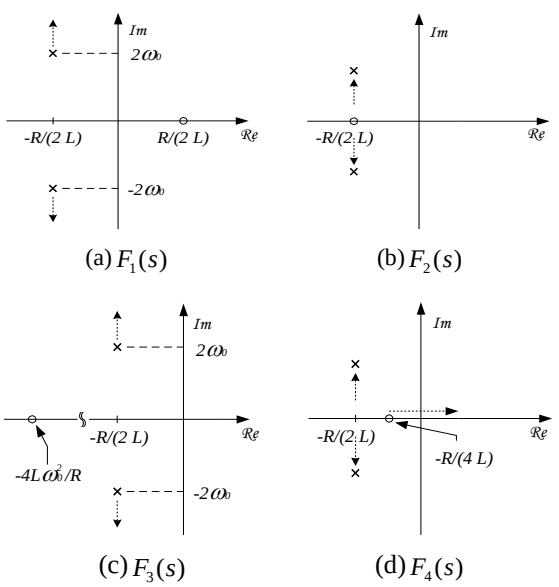

Fig. 3. Zeros and poles of the cross-coupled transfer function.

Input components of $I_1(s)$ and $I_2(s)$ are $V_1(s)$ and $V_2(s)$. In order to observe the response characteristics of the $I_1(s)$ and $I_2(s)$, the poles and zeros of $F_1(s), F_2(s), F_3(s)$, and $F_4(s)$ are plotted in the S domain as the below.

The real parts of all the poles have the same value and the imaginary parts increase as the operating frequency increases as shown in the Fig.3. The poles are related to the response and stability of the system. When the poles have the same real value, the dominant poles are determined by the poles with the lower natural frequency. Response can be mainly determined by dominant poles, $F_2(s)$ and $F_4(s)$.

Generally the resonant inverters have high Q(quality factor) value for high efficiency and controllability. And the operation range of resonant inverters is between the resonant frequency and upper half-power frequency. These conditions can be expressed as following.

$$Q = \frac{\omega_0 L}{R} \rangle\rangle 1 \tag{15}$$

$$1 \le \frac{\omega_C}{\omega_0} \le (1 + \frac{1}{2Q}) \tag{16}$$

Under the conditions (15) and (16), the coefficient A, C, E and F is satisfied with $8\omega_c\omega_o \rangle\rangle R^2/L^2$. Therefore (13) and (14) can be simplified as following.

$$I_1(s) \approx \frac{1}{2L}\left\{\frac{s-\frac{R}{2L}\frac{\omega_c}{\omega_o}}{M_1(s)} + \frac{s+\frac{R}{2L}\frac{\omega_c}{\omega_o}}{M_2(s)}\right\}V_1(s) - \frac{R}{4\omega_o L^2}\left\{\frac{s+\frac{2L}{R}(\omega_o{}^2+\omega_c\omega_o)}{M_1(s)} - \frac{s+\frac{2L}{R}(\omega_o{}^2-\omega_c\omega_o)}{M_2(s)}\right\}V_2(s) \tag{17}$$

$$I_2(s) \approx -\frac{1}{2L}\left\{\frac{s-\frac{R}{2L}\frac{\omega_c}{\omega_o}}{M_1(s)} + \frac{s+\frac{R}{2L}\frac{\omega_c}{\omega_o}}{M_2(s)}\right\}V_2(s) - \frac{R}{4\omega_o L^2}\left\{\frac{s+\frac{2L}{R}(\omega_o{}^2+\omega_c\omega_o)}{M_1(s)} - \frac{s+\frac{2L}{R}(\omega_o{}^2-\omega_c\omega_o)}{M_2(s)}\right\}V_1(s) \tag{18}$$

Considering the operating conditions of resonant inverters, (15) and (16), the coefficients of $1/2L$ and $R/4\omega_o L^2$ have a relationship of $1/2L \rangle\rangle R/4\omega_o L^2$. (17) and (18) can be simplified again as below.

$$I_1(s) \approx \frac{1}{2L}\left\{\frac{s-\frac{R}{2L}\frac{\omega_c}{\omega_o}}{M_1(s)} + \frac{s+\frac{R}{2L}\frac{\omega_c}{\omega_o}}{M_2(s)}\right\}V_1(s) \tag{19}$$

$$I_2(s) \approx -\frac{1}{2L}\left\{\frac{s-\frac{R}{2L}\frac{\omega_c}{\omega_o}}{M_1(s)} + \frac{s+\frac{R}{2L}\frac{\omega_c}{\omega_o}}{M_2(s)}\right\}V_2(s) \tag{20}$$

According to (19) and (20), $I_1(s)$ and $I_2(s)$ are affected by the input of $V_1(s)$ and $V_2(s)$, respectively. From (19) and (20), $M_1(s)$ and $M_2(s)$ can be expressed as $s^2 + \frac{R}{L}s + \frac{R^2}{4L^2} + (\omega_c + \omega_o)^2$ and $s^2 + \frac{R}{L}s + \frac{R^2}{4L^2} + (\omega_c - \omega_o)^2$, respectively. The poles of $M_1(s)$ and $M_2(s)$ are obtained as below.

$$s_{1,2} = -\frac{R}{2L} \pm \frac{1}{2}\sqrt{\frac{R^2}{L^2} - 4\left(\frac{R^2}{4L^2} + (\omega_c + \omega_o)^2\right)} = -\frac{R}{2L} \pm j(\omega_c + \omega_o)^2 \tag{21}$$

$$s_{3,4} = -\frac{R}{2L} \pm \frac{1}{2}\sqrt{\frac{R^2}{L^2} - 4\left(\frac{R^2}{4L^2} + (\omega_c - \omega_o)^2\right)} = -\frac{R}{2L} \pm j(\omega_c - \omega_o)^2 \tag{22}$$

When $\omega_c = \omega_o$, the poles of $M_1(s)$ and $M_2(s)$ are $s_{1,2} = -\frac{R}{2L} \pm j2\omega_o{}^2$ and $s_{3,4} = -\frac{R}{2L}$. Therefore, the real part of each pole is the same but, the imaginary part is different. The pole with the lower imaginary part dominantly affects the response. Accordingly, the dominant poles are s_3 and s_4. Under the condition (15) and (16), ω_c/ω_o can be assumed as $\omega_c/\omega_o \approx 1$. Thus, (19) and (20) can be simplified by the above conditions.

$$I_1(s) \approx \frac{1}{2L}\left\{\frac{s+\frac{R}{2L}}{\left(s+\frac{R}{2L}\right)^2 + (\omega_c - \omega_o)^2}\right\}V_1(s) \tag{23}$$

$$I_2(s) \approx -\frac{1}{2L}\left\{\frac{s+\frac{R}{2L}}{\left(s+\frac{R}{2L}\right)^2+(\omega_c-\omega_o)^2}\right\}V_2(s) \tag{24}$$

The frequency-variable ω_m builds the real part of voltage $V_1(s)$ and the imaginary part of voltage $V_2(s)$ as (8). The even function of $V_1(s)$ has AC and DC components at limited value of β/ω_m. And the odd function of $V_2(s)$ has only an AC component. So $I_1(s)$ induced from $V_1(s)$ becomes the dominant part. And $I_2(s)$ induced from $V_2(s)$ can be negligible since the high frequency AC component is filtered by the system poles. So we can assume $I(s) \approx I_1(s)$.

The steady state current is defined as I_{DC} and can be expressed as following.

$$I_{DC} = \frac{V_s}{R\sqrt{1+Q^2\left(\frac{\omega_c}{\omega_o}-\frac{\omega_o}{\omega_c}\right)^2}} \tag{25}$$

The magnitude of the I_{DC} is determined by the typical RLC resonance curve shown in Fig. 4.

The envelope of the output current as a function of the operating frequency is defined as a constant K_o and expressed as below.

$$\frac{\Delta I_{DC}}{\Delta \omega_c} = K_o \tag{26}$$

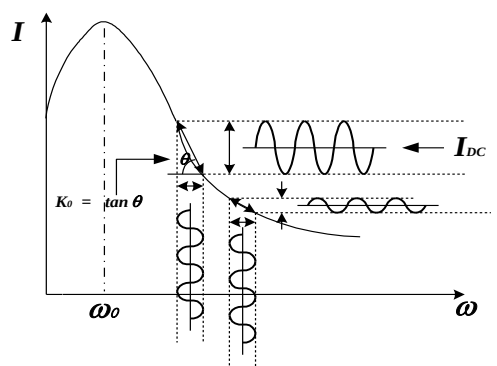

Fig. 4. RLC series resonant curve.

Therefore, K_o can be obtained as following.

$$K_o = \frac{-\left(\omega_c{}^4-\omega_o{}^4\right)V_s}{L\left\{\omega_c{}^4+\left(\left(\frac{R}{L}\right)^2-2\omega_o{}^2\right)\omega_c{}^2+\omega_o{}^4\right\}^{3/2}} \tag{27}$$

In order to obtain the steady state gain, let $s=0$ in (23) and the following equation can be derived.

$$I(0) = \left.\frac{s+\frac{R}{2L}}{\left(s+\frac{R}{2L}\right)^2+(\omega_c-\omega_o)^2}\right|_{s=0} = \frac{\frac{R}{2L}}{\frac{R^2}{4L^2}+(\omega_c-\omega_o)^2}$$

$$= \frac{2LR}{R^2+4L^2(\omega_c-\omega_o)^2} \tag{28}$$

The coefficient, satisfying the condition that the DC gain of transfer function is in unity, should be the inverse of $I(0)$. The product of the magnitude, K_0 and the inverse of $I(0)$ can be expressed as new coefficient K_1, shown in following (29).

$$K_1 = \left(\frac{2LR}{R^2+4L^2(\omega_c-\omega_o)^2}\right)^{-1}\cdot\frac{-\left(\omega_c{}^4-\omega_o{}^4\right)V_s}{L\left\{\omega_c{}^4+\left(\left(\frac{R}{L}\right)^2-2\omega_o{}^2\right)\omega_c{}^2+\omega_o{}^4\right\}^{3/2}} \tag{29}$$

The proposed linear transfer function of the frequency-controlled resonant inverter is defined in Fig. 5.

4. Simulation and Experimental Results

Matlab simulation of the proposed transfer function is performed. The simulation parameters are shown in Table 1.

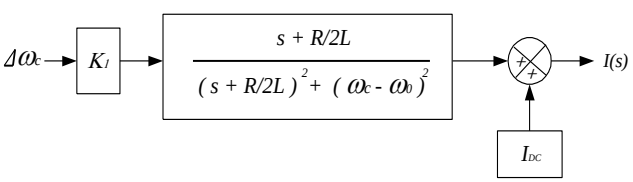

Fig. 5. The block diagram of the proposed inear transfer function.

Table 1. Simulation parameters.

Parameter	Value
Input voltage : V_s	47[V]
Load : R_L	10[Ω]
Inductor : L	0.72[mH]
Capacitor : C	0.09[uF]
Resonant frequency : f_o	19.8[kHz]

The step responses around the resonant frequency were simulated under the condition of frequency change from 20.2kHz to 20kHz and 20.7kHz to 20.5kHz. Furthermore, the step response in the vicinity of the upper half-power frequency was also simulated by the application of frequency change from 21.2kHz to 21kHz. The simulation results are shown in Fig. 6.

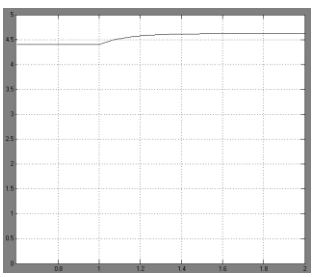

(a) Step response(20.2kHz→20kHz)
(0.5A/div, 0.2ms/div)

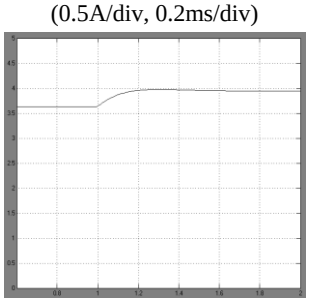

(b) Step response(20.7kHz→20.5kHz)
(0.5A/div,0.2ms/div)

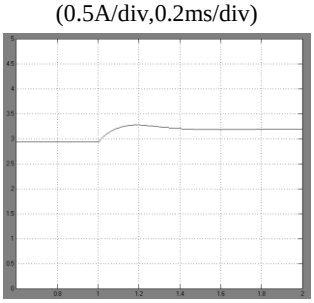

(c) Step response(21.2kHz→21kHz)
(0.5A/div, 0.2ms/div).

Fig. 6. Simulation results.

Experimental setup was built and the controller was implemented using dsPIC30f2020 from Microchip in order to verify the feasibility of the proposed transfer function. The experiment was performed under the same condition as that of the Matlab simulation. The experimental configuration is shown in Fig. 7.

The step response, obtained from the experiment performed under the condition of frequency change from 20.2kHz to 20kHz, was illustrated in Fig. 8. The step responses determined from both the experiment and simulation were compared in Fig. 8. The step responses determined from both the experiment and simulation performed under the condition of frequency change from 20.7kHz to 20.5kHz were shown in Fig. 9.

The measured and simulated step responses monitored around the resonant frequency perfectly coincide.

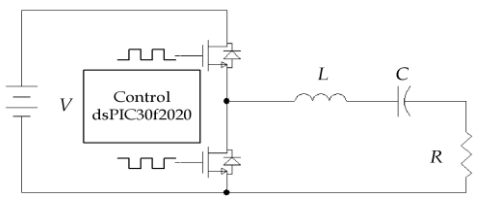

Fig. 7. The configuration of the experimental setup.

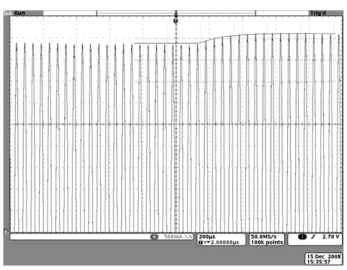

Fig. 8. Experimental waveforms: step response (20.2kHz→ 20kHz) (0.5A/div, 0.2ms/div).

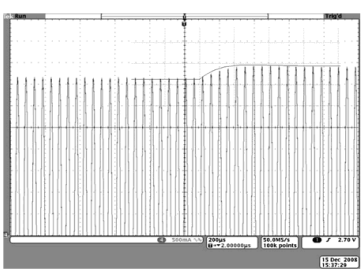

Fig. 9. Experimental waveforms: step response (20.7kHz→ 20.5kHz) (0.5A/div, 0.2ms/div).

The step response in the vicinity of the upper half-power frequency was also experimented by the application of frequency change from 21.2kHz to 21kHz. The response is shown in Fig. 10. The bode plots of the transfer function and experimental result at the operating point 20.6kHz are shown in Fig.11.

The difference between the simulated and experimental responses is observed in the transient region as the operating frequency gets close to the upper half-power frequency. The difference between the experiment and simulation in the step response is due to the linear transfer function model. However, the rising time and settling time of the experiment and simulation agree with each other. Therefore, the frequency controlled resonant inverter can be modeled as the proposed 2^{nd} order linear transfer function. The precise agreement between the simulation and experimental results shows that the proposed linear transfer function can predict the envelope dynamics accurately.

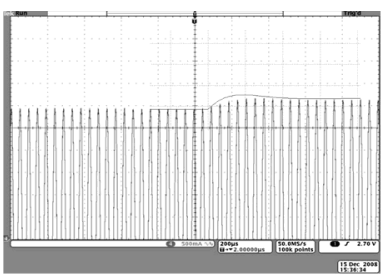

Fig. 10. Experimental waveforms: step response (21.2kHz→ 21kHz) (0.5A/div, 0.2ms/div).

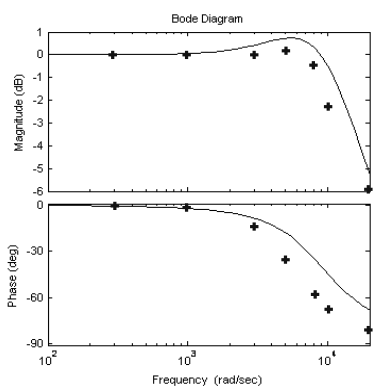

Fig. 11. Bode plots of the transfer function and experimental result at the operating point 20.6kHz.

5. Conclusions

This paper presents a novel 2^{nd} order linear transfer function of frequency-controlled resonant inverters based on behavior analysis of the pole locations that facilitate a simple and intuitive linear transfer function. The modulation input voltage and the circuit have been equivalently modeled into the cross-coupled equivalent circuits using the complex phasor transform. The cross-coupled state space equation has been established from the equivalent circuits. It has been simplified into the linear transfer function which was driven by observing the pole diagrams and the behavior of the circuit.

The feasibility and validity of the proposed method were verified by means of computer simulations and experimental results. The simulation results and experiments show that the proposed linear transfer function can predict the current envelope dynamics accurately at between the resonant frequency and upper half-power frequency.

References

[1] E.X. Yang, F.C. Lee, and M.M. Jovanovic, "Small-signal modeling of series and parallel resonant converters," *in Proc. of IEEE APEC'92*, pp. 785-792, 1992.

[2] R.L. Steigerwald, "High-frequency resonant transistor DC-DC Converters," *IEEE Trans. Ind. Electron.*, Vol. IE-31, pp. 182-190, 1984.

[3] B.C. Pollard and R.M. Nelms, "Using the series parallel resonant converter in capacitor charging applications," *in Proc. of IEEE APEC'92*, pp. 731-737, 1992.

[4] E. Deng and S. Cuk, "Negative incremental impedance and stability of fluorescent lamp," *in Proc. of IEEE APEC'97*, pp. 1050-1056, 1997.

[5] S. Ben-Yaakov, S. Glozman, and R. Rabinovici, "Envelope Simulation by SPICE-Compatible Models of Linear Electric Circuits Driven by Modulated Signals," *IEEE Trans. Indus.* Appli., Vol. 37 No.2, pp.527-533, 2001.

[6] S. Ben-Yaakov, M. Shvartsas, and S. Glozman, "Statics and dynamics of fluorescent lamps operating at high frequency: Modeling and simulation," *in Proc. of IEEE APEC'99*, pp. 467-472, 1999.

[7] C. T. Rim and G. H. Cho, "Phasor transformation and its application to the DC/AC analyzes of frequency phase-controlled series resonant converter(SCR)," *IEEE*

Trans. Power Electron., Vol. 5, pp. 201-211, 1990.

[8] A. F. Witulski and R. W. Erickson, "Small signal ac equivalent circuit modeling of the series resonant converter," *in Proc. of IEEE PESC'87*, pp. 693-704, 1987.

[9] V. Vorperian, "Approximate small-signal analysis of the series and the parallel resonant converters," *IEEE Trans, On Power Electronics*, Vol. 4, pp. 15-24, 1989.

[10] I.J. Pitel, "Phase-modulated resonant power conversion techniques for high-frequency link inverters," *IEEE Trans. Ind. Appl.*, Vol. IA-22, No. 6, pp. 1044-1051, 1986.

[11] Y. Yin, R. Zane, R. Erickson, and J. Glaser, "Dynamic analysis of frequency-controlled electronic ballasts," *in Conf. Rec. IEEE Ind. Appl. 37th IAS annual meeting*, pp. 685-691, 2002.

[12] Zhongming Ye, Praveen K.jain and Paresh C. Sen, "Modeling of High Frequency Resonant Inverter System in Phasor Domain for Fast Simulation and Control Design," *in Proc. of IEEE PESC'08*, pp. 2090-2096, 2008.

[13] E. Deng, "Negative Incremental Impedance of Fluorescent Lamp," Ph.D. Thesis, California Institute of Technology, Pasadena, 1995.

Mu-Ho Han was born in Daegu, Korea in 1969. He received the B.S. and M.S. degrees in Electronics Engineering from Kyungpook National University, Korea, in 1992 and 1994, respectively. Since 1994, he has been with Research Institute of Science and Technology, where he is currently a senior researcher. His research interests are in the areas of modeling and control of induction heating and power electronics.

Chi-Hwan Lee was born in Daegu, Korea, in 1961. He received the B.S. degree from Yeoungnam University in 1984 and M.S. and Ph.D degrees in Electronics Engineering from Kyungpook National University, Korea, in 1988 and 1994, respectively. Since 1998, he has been with the Department of Electronics Engineering, Uiduk University, where he is currently an associate professor. His research interests are in the areas of control of resonant inverters and power electronics.

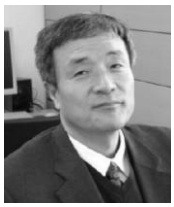

Woo-Hyen Kwon was born in Korea on June 22, 1953. He received the M.S. and Ph.D. degrees from the Korea Advanced Institute of Science and Technology(KAIST). Seoul, Korea, in 1979 and 1993, respectively. He has been with the School of Electrical Engineering and Computer Science in the Kyungpook National University since 1979, where he is now a Professor. His research interests are in the area of static power converters and drives, and computer applied control systems.